

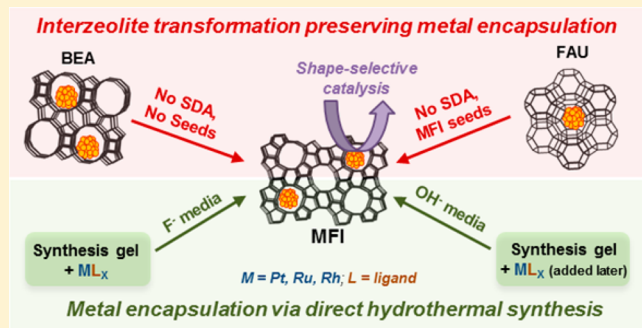
Encapsulation of Metal Clusters within MFI via Interzeolite Transformations and Direct Hydrothermal Syntheses and Catalytic Consequences of Their Confinement

Sarika Goel, Stacey I. Zones,*† and Enrique Iglesia*

Department of Chemical and Biomolecular Engineering, University of California at Berkeley, Berkeley, California 94720, United States

Supporting Information

ABSTRACT: The encapsulation of metal clusters (Pt, Ru, Rh) within MFI was achieved by exchanging cationic metal precursors into a parent zeolite (BEA, FAU), reducing them with H₂ to form metal clusters, and transforming these zeolites into daughter structures of higher framework density (MFI) under hydrothermal conditions. These transformations required MFI seeds or organic templates for FAU parent zeolites, but not for BEA, and occurred with the retention of encapsulated clusters. Clusters uniform in size (1.3–1.7 nm) and exposing clean and accessible surfaces formed in BEA and FAU zeolites; their size remained essentially unchanged upon transformation into MFI. Encapsulation selectivities, determined from the relative hydrogenation rates of small (toluene) and large (alkyl arenes) molecules and defined as the ratio of the surface areas of all the clusters in the sample to that of external clusters, were very high (8.1–40.9) for both parent and daughter zeolites. Encapsulation into MFI via direct hydrothermal syntheses was unsuccessful because metal precursors precipitated prematurely at the pH and temperatures required for MFI synthesis. Delayed introduction of metal precursors and F[−] (instead of OH[−]) as the mineralizing agent in hydrothermal syntheses increased encapsulation selectivities, but they remained lower than those achieved via interzeolite transformations. These interconversions provide a general and robust strategy for encapsulation of metals when precursors can be introduced via exchange into a zeolite that can be transformed into target daughter zeolites with higher framework densities, whether spontaneously or by using seeds or structure-directing agents (SDA).



1. INTRODUCTION

Zeolites are ordered microporous aluminosilicates with well-defined crystal structures. Voids of molecular dimensions allow zeolites to catalyze chemical reactions with unique reactivities and selectivities.^{1–6} Synthesis protocols for encapsulating metals^{7–18} within zeolites can expand the diversity of catalytic chemistries, made possible by the ability of microporous solids to select reactants, transition states, and products based on their molecular size and shape, and to protect active sites from larger species that act as poisons by titrating active sites. General protocols for encapsulating metal clusters within zeolites of different void size and geometry can be used to tailor or select zeolite structures for specific catalytic applications; the methods include ion exchange,^{10–12} incipient wetness,^{10,12} and incorporation of metal precursors during synthesis.^{9,10,13–18}

The apertures within small and medium-pore zeolites preclude post-synthetic encapsulation protocols via ion-exchange from aqueous media, which require the migration of solvated metal-oxo oligomers that cannot diffuse through the small apertures in such zeolites.^{9,13–18} Recently, we have developed encapsulation methods that exploit the use of ligand-stabilized metal precursors to prevent the premature precipitation of metal precursors as colloidal oxyhydroxides at the

high pH and temperatures required for hydrothermal zeolite crystallization.^{15–18} These protocols have led to the successful encapsulation of Pt, Pd, Rh, Ir, Re, and Ag clusters within LTA¹⁷ and Pt, Pd, Ru, and Rh clusters within GIS and SOD.¹⁸ Some zeolites require synthesis temperatures that decompose even ligand-stabilized metal precursors; in such cases, we have enforced encapsulation by first placing metal clusters within zeolites that form at milder conditions (parent structure) and then subjecting the sample to the conditions that convert this parent zeolite to the intended framework (daughter structure), while preserving encapsulation. These protocols have led to the successful encapsulation of Pt and Ru clusters within ANA.¹⁸

MFI (ZSM-5) is a medium-pore silica-rich zeolite that typically requires high crystallization temperatures (423–473 K) and pH (>11) for its template-free synthesis; encapsulation in such materials remains inaccessible via procedures involving direct hydrothermal synthesis using ligand-stabilized metal precursors,^{15–18} as well as post-synthesis exchange,¹⁴ except in the case of monovalent or divalent cations. Here, we report a general strategy for the encapsulation of metal clusters within

Received: August 4, 2014

Published: October 14, 2014



Table 1. Initial Synthesis Molar Compositions of the Samples^a

| sample name | parent zeolite (Si/Al) | time of synthesis (h) | additional (SDA/seed) ^b | product phase | yield (%) ^c | product (Si/Al) ^d |
|---------------------|------------------------|-----------------------|------------------------------------|---------------|------------------------|------------------------------|
| MFI _B | BEA(37.5) | 24 | | MFI | 46.4 | 22 |
| MFI _B -T | BEA(37.5) | 24 | TPABr (0.05) ^e | MFI | 47.3 | 35 |
| MFI _B -S | BEA(37.5) | 24 | 10% wt MFI seeds | MFI | 47.1 | 23 |
| Pt/MFI _B | Pt/BEA(37.5) | 30 | | MFI | 47.7 | |
| Ru/MFI _B | Ru/BEA(37.5) | 30 | | MFI | 47.3 | |
| MFI _F | FAU(40) | 40 | | amor. | 75.5 | |
| MFI _F -T | FAU(40) | 40 | TPABr (0.05) ^e | MFI | 57.9 | 33 |
| MFI _F -S | FAU(40) | 40 | 10% wt MFI seeds | MFI | 47.1 | 22 |
| Pt/MFI _F | Pt/FAU(40) | 40 | 10% wt MFI seeds | MFI | 48.5 | 29 |
| Ru/MFI _F | Ru/FAU(40) | 40 | 10% wt MFI seeds | MFI | 56.8 | 25 |
| Rh/MFI _F | Rh/FAU(40) | 40 | 10% wt MFI seeds | MFI | 56.2 | 28 |

^aMolar ratios 0.35 NaOH: 1.0 SiO₂: 0.0133 Al₂O₃: 65 H₂O for transformations of BEA and 0.5 NaOH: 1.0 SiO₂: 0.0125 Al₂O₃; 95 H₂O for FAU at 423 K and excludes the SiO₂ amount of seed materials. ^bseed (wt %) = $\frac{\text{seed material (g)}}{\text{parent zeolite (g)}} \times 100$. ^cyield (%) = $\frac{\text{product (g)}}{\text{parent zeolite (g)} + \text{seed (g)}} \times 100$. ^dAnalyzed by inductively coupled plasma optical emission spectroscopy. ^eValues in parentheses show molar composition of TPABr relative to SiO₂.

MFI by exploiting interzeolite transformations of BEA or FAU zeolites (parent structures) into MFI zeolite (daughter structure), without organic SDA, and describe the catalytic consequences of the selective encapsulation of metal clusters (Pt, Ru, Rh) within the void spaces of MFI frameworks.

Interzeolite transformations^{19,20} provide a general and convenient route for the encapsulation of clusters within microporous solids in those cases for which the successful placement of precursors can be accomplished within a parent zeolite structure via post-synthesis exchange or during hydrothermal crystallization. This parent structure, containing metal clusters within its microporous voids, can then be recrystallized without loss of encapsulation into a daughter structure of higher framework density, in this case MFI, for which more direct methods of encapsulation are unavailable or impractical. We also report evidence for the factors that influence the encapsulation selectivity in direct hydrothermal synthesis protocols. Such direct methods lead to low encapsulation yields, making interzeolite transformations the method of choice for the encapsulation of metal clusters within MFI.

2. EXPERIMENTAL SECTION

Methods. 2.1. *Reagents and Materials.* Fumed SiO₂ (Cab-O-Sil, HS-5, 310 m² g⁻¹), NaOH (99.995%, Sigma-Aldrich), FAU (CBV780, Zeolyst, H-FAU, Si/Al = 40), BEA (CP811E-75, Zeolyst, H-BEA, Si/Al = 37.5), tetrapropylammonium bromide (TPABr; 98%, Sigma-Aldrich), NaAlO₂ (anhydrous, Riedel-de Haen, technical), Al(NO₃)₃·9H₂O (>98%, Strem Chemical), NH₄F (>98%, Fluka), tetraethyl orthosilicate (TEOS; 98%, Sigma-Aldrich), [Pt(NH₃)₄](NO₃)₂ (99.99%, Alfa Aesar), [Rh(NH₂CH₂CH₂NH₂)₃]Cl₃·3H₂O (>99.5%, Aldrich), RuCl₃ (45–55% wt Ru, Sigma-Aldrich), Ludox AS-30 colloidal silica (30% wt suspension in H₂O, Sigma-Aldrich), [Ru(NH₃)₆]Cl₃ (98%, Aldrich), toluene (>99.9%, Aldrich), 1,3,5-trimethylbenzene (98%, Aldrich), He (99.999%, Praxair), air (99.999%, Praxair), 0.5% O₂/He (99.999%, Praxair), 9% H₂/He (99.999%, Praxair), and H₂ (99.999%, Praxair) were used as received.

2.2. *Synthesis Procedures.* 2.2.1. *MFI Seed Crystals.* In a typical synthesis, 649 g of water, 740 g of 1 mol dm⁻³ NaOH (Baker Reagent), and 98 g of tetrapropylammonium bromide (Kodak Chemicals) were added to 872 g of Ludox AS-30 colloidal SiO₂ (Dupont). The synthesis mixture was then transferred into a Hastelloy-lined stainless steel autoclave (3.8 dm³), pressure tested, and held at 423 K for 4 days in a convection oven under rotation (78 rpm). After 4 days, the autoclave was cooled, and the resulting solid was collected by filtration and washed with deionized water (17.9 MΩ resistivity) until the rinse liquids reached a pH of 7–8. The resulting

product was crystalline MFI (confirmed by powder X-ray diffraction (XRD)) with Si/Al ~ 300 (by inductively-coupled plasma atomic emission spectroscopy (ICP-AES) analysis) and ~6 μm sized zeolite crystals (by transmission electron microscopy (TEM)).

2.2.2. *Synthesis of MFI via Interzeolite Transformations of Parent BEA or FAU Zeolites.* In a typical synthesis, zeolite BEA (Si/Al = 37.5) or FAU (Si/Al = 40) was added (1.0 g) to an aqueous NaOH solution, into which the MFI seed crystals or structure-directing agents (TPABr) were added to prepare final mixtures with molar compositions listed in Table 1. These mixtures were placed within sealed polypropylene containers (Nalgene, 125 cm³) and homogenized by vigorous magnetic stirring (400 rpm; IKA RCT Basic) for 1 h at ambient temperature. The mixture was then transferred into a Teflon-lined stainless steel autoclave and held at 423 K for 24–40 h under static conditions. The resulting solids were collected by filtration through a fritted disc Buchner filter funnel (Chemglass, 150 mL, F) and washed with deionized water (17.9 MΩ resistivity) until the rinse liquids reached a pH of 7–8. The sample was heated in convection oven at 373 K overnight and the solid yield of the resulting product was defined as

$$\text{yield (\%)} = \frac{\text{product (g)}}{\text{parent zeolite (g)} + \text{seed (g)}} \times 100 \quad (1)$$

The resulting product was then treated in flowing air (1.67 cm³ g⁻¹ s⁻¹) to 623 K at 0.03 K s⁻¹ and held at this temperature for 3 h. The samples after treatment were denoted as MFI_B, MFI_B-T, and MFI_B-S when synthesized from BEA, and MFI_F, MFI_F-T, and MFI_F-S when synthesized from FAU, in the direct, template-assisted and seed-assisted transformations, respectively.

2.2.3. *Encapsulation of Metal Clusters within BEA and FAU by Ion Exchange Method.* Parent zeolites (FAU or BEA) were added to an aqueous solution of NaCl (>99.0%, Sigma-Aldrich, 1 g zeolite per 100 cm³ 1 M solution) while stirring (400 rpm; IKA RCT Basic) at 353 K for 8 h. The exchange was repeated a total of three times to yield Na-Zeolite, and the solids were recovered by filtration, washed with deionized water and dried overnight in convection oven at 373 K and the resulting materials were used for subsequent ion exchange with metals. Metals (M = Pt, Ru, Rh) encapsulated within BEA or FAU were prepared by ion exchange from aqueous solutions of [Pt(NH₃)₄](NO₃)₂, [Rh(NH₂CH₂CH₂NH₂)₃]Cl₃·3H₂O, or [Ru(NH₃)₆]Cl₃ (10:1 mass ratio of H₂O/zeolite, to achieve ~1% wt metal content) at 353 K by magnetic stirring (400 rpm; IKA RCT Basic) for 8 h. The solids obtained were collected by filtration through a fritted disc Buchner filter funnel (Chemglass, 150 mL, F) and washed with deionized water until the rinse liquids reached a pH of 7–8. These samples were then heated in convection oven at 373 K overnight and treated in flowing air (1.67 cm³ g⁻¹ s⁻¹) to 623 K at 0.03 K s⁻¹ and held for 3 h; the metal precursors were then exposed to a flow of 9% H₂/He (1.67 cm³ g⁻¹ s⁻¹) and heated to 573 K at 0.03 K

s^{-1} and held for 2 h. After this treatment, the samples were passivated in 0.5% O₂/He flow (1.67 cm³ g⁻¹ s⁻¹) for 1 h at room temperature before exposure to ambient air. The resulting samples after treatment were denoted as M/BEA and M/FAU (M = Pt, Ru, Rh), synthesized from BEA and FAU, respectively.

2.2.4. Encapsulation of Metal Clusters within MFI via Interzeolite Transformations of Parent BEA. The encapsulation of metal clusters within MFI was achieved by interzeolite transformations of M/BEA (M = Pt, Ru), using M/BEA samples as parent zeolites. M/BEA (M = Pt, Ru) samples (1.0 g) were added to an aqueous NaOH solution (0.35 NaOH: 1.0 SiO₂: 0.0133 Al₂O₃: 65 H₂O) to prepare mixtures with molar compositions listed in Table 1. These mixtures were placed within sealed polypropylene containers (Nalgene, 125 cm³) and homogenized by vigorous magnetic stirring (400 rpm; IKA RCT Basic) for 1 h at ambient temperature. The mixture was then transferred into a Teflon-lined stainless steel autoclave and held at 423 K under static conditions for 40 h. The resulting solids were collected by filtration through a fritted disc Buchner filter funnel (Chemglass, 150 mL, F) and washed with deionized water until the rinse liquids reached a pH of 7–8. These samples were heated in ambient air at 373 K overnight and then treated in flowing air (1.67 cm³ g⁻¹ s⁻¹) to 673 K at 0.03 K s⁻¹ and held for 3 h; the metal precursors were then exposed to a flow of 9% H₂/He (1.67 cm³ g⁻¹ s⁻¹) and heated to 623 K at 0.03 K s⁻¹ and held for 2 h. After this treatment, the samples were passivated in 0.5% O₂/He flow (1.67 cm³ g⁻¹ s⁻¹) for 1 h at room temperature before exposure to ambient air. The resulting samples after treatment were denoted as M/MFI_B (M = Pt, Ru), synthesized via transformations of M/BEA parent zeolites.

2.2.5. Encapsulation of Metal Clusters within MFI via Interzeolite Transformations of Parent FAU. The encapsulation of metal clusters within MFI was also achieved by interzeolite transformations of M/FAU (M = Pt, Ru, Rh), using M/FAU samples as parent zeolites. M/FAU (M = Pt, Ru, Rh) samples (1.0 g) were added to an aqueous NaOH solution (0.5 NaOH: 1.0 SiO₂: 0.0125 Al₂O₃: 95 H₂O) along with 10% wt MFI seeds (% wt based on parent FAU) to prepare mixtures with molar compositions listed in Table 1. All of the subsequent synthesis and treatment steps were identical to those described for M/MFI_B samples synthesized via interzeolite transformation of M/BEA samples. The resulting samples after treatment were denoted as M/MFI_F (M = Pt, Ru, Rh), synthesized via transformations of M/FAU parent zeolites.

2.2.6. Encapsulation of Metal Clusters within MFI via Direct Hydrothermal Syntheses. The encapsulation of metal clusters within MFI was studied at various synthesis conditions, shown in Table 5, during hydrothermal syntheses, adapted from Refs 21 and 22. Synthesis gels with molar compositions shown in Table 5 were prepared. In a typical experiment, the alumina source (NaAlO₂ or Al(NO₃)₃·9H₂O) and NaOH were dissolved in deionized H₂O (17.9 MΩ resistivity) and mixed with SiO₂ source (Ludox AS-30 or TEOS) and other necessary reagents (e.g., TPABr, NH₄F, or HF) to prepare the mixtures of molar composition shown in Table 5. The resultant gel was transferred into a 125 cm³ polypropylene container (Nalgene), sealed, and homogenized by magnetic stirring at 400 rpm (IKA RCT Basic) for 1 h at ambient temperature. The mixture was then transferred into a Teflon-lined stainless steel autoclave and held at desired crystallization temperature under static conditions for a total synthesis time shown in Table 5. The resulting solids were collected by filtration through a fritted disc Buchner filter funnel (Chemglass, 150 mL, F) and washed with deionized water (17.9 MΩ resistivity) until the rinse liquids reached a pH of 7–8. All of the subsequent treatment steps were identical to those described for M/MFI_B samples synthesized via interzeolite transformations of M/BEA samples.

2.2.7. Silica-Supported Metal Clusters. The metal clusters dispersed on SiO₂ (Davisil, grade 646, 300 m² g⁻¹) were prepared by the incipient wetness impregnation methods¹⁶ using aqueous solutions of the same metal precursors as for the ion-exchanged zeolites (BEA or FAU). Silica supported metal samples were also treated using the same procedures as the ion-exchanged BEA or FAU samples (subsection 2.2.3).

2.3. Structural Characterization. The identity and phase purity of product zeolites as well as the absence of large metal clusters were demonstrated by powder X-ray diffraction (Cu K α radiation $\lambda = 0.15418$ nm, 40 kV, 40 mA, Bruker D8 Advance). Diffractograms were measured for 2 θ values of 5–50° at 0.02° intervals with a 2 s scan time. Si, Al, Na, and metal (Pt, Ru, or Rh) contents were measured by inductively coupled plasma atomic emission spectroscopy (IRIS Intrepid spectrometer; Galbraith Laboratories). The dispersion of the metal clusters was determined by H₂ chemisorption uptakes using volumetric methods. Samples were heated to 623 K at 0.03 K s⁻¹ in flowing H₂ (1.67 cm³ s⁻¹ g⁻¹) and held for 1 h and then evacuated for 1 h at 623 K to remove any weakly adsorbed hydrogen before being cooled to 298 K. Hydrogen chemisorption uptakes were measured at 298 K and 5–50 kPa of H₂ on metal containing samples. Dispersions were determined from the difference between total and irreversible H₂ uptakes, extrapolated to zero pressure, using a 1.0 H/M_{surface} (M = Pt, Ru, Rh) adsorption stoichiometry.²³ Transmission electron microscopy (TEM) images were taken with Philips/FEI Tecnai 12 microscope operated at 120 kV. Before TEM analysis, the samples were suspended in ethanol and dispersed onto ultrathin carbon/holey carbon films supported on 400 mesh Cu grids (Ted Pella Inc.). Size distributions of metal clusters were determined from measuring more than 300 clusters for each sample. Surface-averaged cluster diameters, d_{TEM} ,²³ were calculated using

$$d_{\text{TEM}} = \frac{\sum n_i d_i^3}{\sum n_i d_i^2} \quad (2)$$

where n_i is the number of clusters having a diameter d_i . TEM-derived size distributions were also used to calculate the dispersity index (DI) of the metal clusters. The DI value is given by surface-averaged diameter (d_{TEM} ; eq 2) divided by the number-averaged diameter ($d_n = \sum n_i d_i / \sum n_i$).²⁴

$$\text{dispersity index (DI)} = \frac{d_{\text{TEM}}}{d_n} = \frac{\left(\frac{\sum n_i d_i^3}{\sum n_i d_i^2} \right)}{\left(\frac{\sum n_i d_i}{\sum n_i} \right)} \quad (3)$$

This parameter is a measure of the cluster size heterogeneity of metal clusters, with a value of unity reflecting unimodal clusters and values smaller than 1.5 indicating relatively uniform size distributions.^{23–25}

2.4. Catalytic Rate Measurements. Toluene, 1,3,5-trimethylbenzene (1,3,5-TMB), and 1,3,5-triisopropyl benzene (1,3,5-TIPB) hydrogenation rates were measured on catalyst samples diluted with fumed SiO₂ (Cab-O-Sil, HS-5, 310 m² g⁻¹) using a quartz tubular reactor with plug-flow dynamics. Dilution was achieved by intimate mixing at a diluent/catalyst mass ratio of 10, pelletizing, and sieving the granules to retain aggregates of 0.18–0.25 mm diameter. These granules (5–25 mg) were then mixed with acid-washed quartz granules of similar size (Fluka, acid-purified, 1.0 g, 0.18–0.25 mm). Such dilution was used to avoid intrapellet or bed concentration and temperature gradients.

Pre-reduced and passivated samples were treated in flowing H₂ (1.67 cm³ g⁻¹ s⁻¹) by heating to 623 K at 0.03 K s⁻¹ and holding for 1 h prior to measuring hydrogenation rates. Arene hydrogenation rates were measured with 0.35 kPa toluene or 0.26 kPa 1,3,5-TMB or 0.15 kPa 1,3,5-TIPB and 100 kPa H₂ at 473 K. Toluene (0.59 nm kinetic diameter²⁶), but not 1,3,5-TMB (0.74 nm kinetic diameter²⁷) for MFI (~0.55 nm aperture²⁸) and 1,3,5-TIPB (0.84 nm kinetic diameter²⁷) for BEA (~0.70 nm aperture²⁸) and FAU (0.74 nm aperture²⁸), can diffuse through the apertures of zeolites and access active sites contained within the zeolitic voids. Rates are reported as turnover rates, defined as hydrogenation rates normalized by the number of surface metal atoms determined from hydrogen chemisorption uptakes. Reactant and product concentrations were measured by gas chromatography (Agilent 6890GC) using a methyl-silicone capillary column (HP-1; 50 m × 0.25 mm, 0.25 μm film thickness) connected to a flame ionization detector. Quartz, fumed SiO₂, or metal-free zeolites did not give detectable hydrogenation rates for any of these reactants, and measured rates did not depend on the extent of dilution

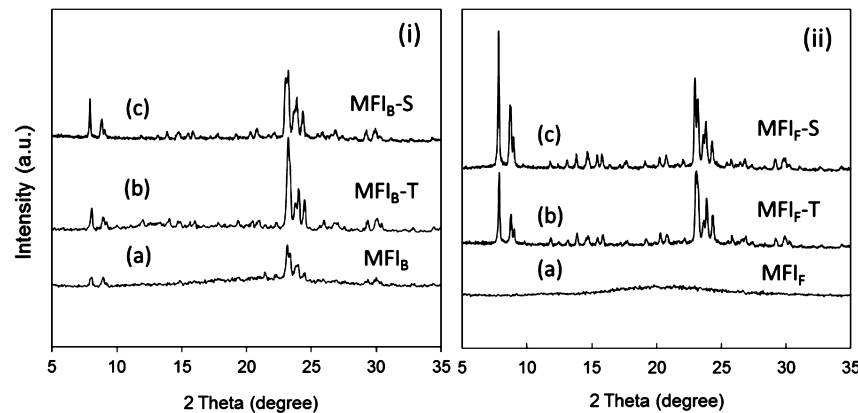


Figure 1. X-ray diffraction patterns of MFI products synthesized from (i) BEA ($\text{Si}/\text{Al} = 37.5$) and (ii) FAU ($\text{Si}/\text{Al} = 40$) parent zeolites via (a) direct, (b) template-assisted (using TPABr), and (c) seed-assisted transformations (using MFI seeds). Syntheses were carried out at molar ratio 0.35 NaOH : 1.0 SiO_2 : 0.0133 Al_2O_3 : 65 H_2O for 24 h from parent BEA and 0.5 NaOH : 1.0 SiO_2 : 0.0125 Al_2O_3 : 95 H_2O for 40 h from parent FAU at 423 K (Table 1). Product yields are shown in Table 1.

or on time on stream for any of the catalysts, consistent with absence of temperature or concentration gradients and of detectable deactivation.

3. RESULTS AND DISCUSSION

The encapsulation of monovalent and divalent cations within medium-pore zeolites, such as MFI, can be achieved by post-synthesis methods involving aqueous or vapor phase exchange or even incipient wetness impregnation.^{10–12} These methods fail, however, for trivalent and higher-valent metals (e.g., Ru, Rh, Ir, etc.), which cannot enter medium-pore and small-pore zeolites as solvated cations or anions, because of their larger size and their extended charge-balancing double-layer, or even as volatile complexes.^{13–18} Thus, the encapsulation of higher-valent metal precursors within these materials requires that precursors be placed and retained within microporous frameworks during their hydrothermal synthesis and subsequent thermal treatment. In such cases, interzeolite transformations can provide an alternate synthetic route for the encapsulation of metal clusters within zeolitic voids, when a zeolite of lower framework density and larger apertures can be used to initially contain metal precursors or clusters; such materials can then be subsequently converted to a zeolite with higher framework density and smaller apertures while retaining the encapsulated species within the zeolitic voids.

Interzeolite transformations^{19,20} can convert structures with lower framework densities into those with higher framework densities, which tend to be thermodynamically more stable. These interconversions may avoid costly organic templates and/or decrease crystallization times; they may also provide more general routes for encapsulating clusters within those zeolites that would otherwise require synthesis temperatures that lead to the decomposition of metal precursors during hydrothermal syntheses, even for precursors containing protecting ligands. Thermodynamics typically allow transformations that increase the zeolite framework density (FD; reported here as T atoms/nm³,^{28,29} where T stands for Si or Al atoms in the zeolite framework), but not all such processes are kinetically-accessible under the hydrothermal conditions that are required for the synthesis of daughter structures.

BEA (FD 15.3²⁸) and FAU (FD 13.3²⁸) can be recrystallized to zeolites with higher framework densities in aqueous NaOH solution at temperatures above those that cause their own respective crystallizations from amorphous silica–alumina

precursors under hydrothermal conditions (360–400 K). Crystalline MFI (FD 18.4²⁸) samples were successfully synthesized here from BEA, in the presence or absence of MFI seeds or organic structure directing agents (X-ray diffractograms; Figure 1i), using aqueous NaOH solutions (0.35 NaOH : 1.0 SiO_2 : 0.0133 Al_2O_3 : 65 H_2O , Table 1) under autogenous pressures at 423 K. Thus, we conclude that this transformation can occur spontaneously, without significant kinetic hindrance, and even in the absence of MFI seeds or organic structure-directing agents (SDA).

In contrast, FAU to MFI transformations required the presence of either MFI seeds or tetrapropylammonium bromide (TPABr) as SDA (X-ray diffractograms; Figure 1ii) in aqueous NaOH at 423 K under hydrothermal conditions (0.5 NaOH : 1.0 SiO_2 : 0.0125 Al_2O_3 : 95 H_2O , Table 1). In the absence of seeds or SDA, FAU converted to amorphous solids, but MFI crystals were obtained when FAU was transformed in the presence of TPABr (SDA) or MFI seeds (10% wt seeds, ~6 μm seed crystals) (X-ray diffraction pattern; Figure 1iii). These results show that SDA and MFI seeds help to overcome the kinetic hurdles prevalent in the formation of thermodynamically favored MFI structures from parent FAU zeolites.

We note that the framework structures and composite building units (CBU) of the parent BEA and daughter MFI zeolites include a common *mor* structural motif,²⁸ while FAU and MFI lack such a common CBU. It seems plausible, therefore, that a CBU, present in BEA and required to form MFI, remains essentially intact within the BEA-derived intermediates during its conversion to MFI; this CBU may aid the local nucleation of MFI and, in doing so, reduce kinetic hurdles, thus allowing the BEA transformation into MFI to occur without seeds or SDA. As a consequence, BEA to MFI transformations (X-ray diffractograms, Figure 1i), containing *mor* as a common CBU, become kinetically feasible. This common CBU could serve as kinetic mediator^{30,31} for nucleating the daughter structure, suggesting that zeolites containing common CBU elements may be able to overcome kinetic barriers that obstruct their interconversions in the direction dictated by the thermodynamic tendency of zeolites to form structures with greater framework densities. In contrast, SDA moieties or MFI seeds are required to convert parent FAU to product MFI (X-ray diffractograms, Figure 1ii), apparently to

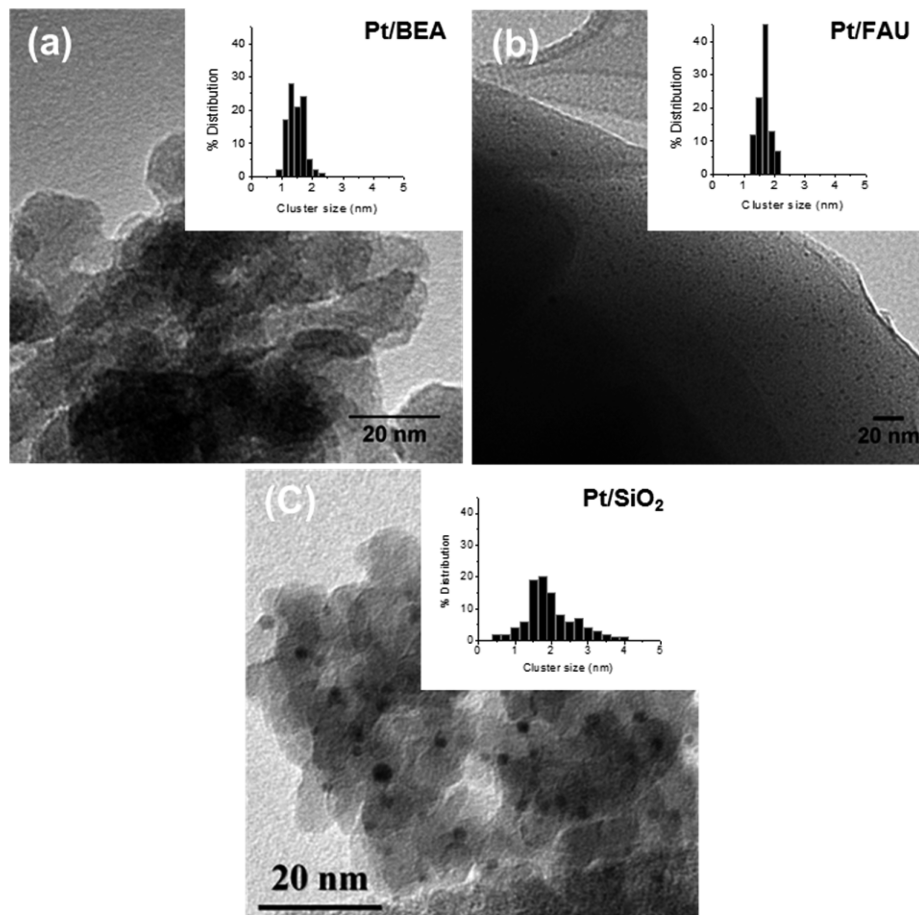


Figure 2. TEM images and metal cluster size distributions of parent (a) BEA and (b) FAU zeolites containing Pt clusters, synthesized by ion exchange methods, and (c) Pt clusters dispersed on SiO_2 , synthesized by incipient wetness impregnation method.

provide the kinetic mediation³² required in the absence of any common CBU.

The solid yields of products (Table 1, eq 1) were 46.4% for BEA to MFI transformation in the absence of SDA or seeds, 47.1% for seed-assisted and 47.3% for template-assisted BEA to MFI transformations and 47.1% for seed-assisted and 57.9% for template-assisted FAU to MFI transformations. These yields (Table 1) and Si/Al ratios of the product zeolites (22–23; Table 1) in direct and seed-assisted transformations indicate that nearly all the Al atoms in the parent BEA ($\text{Si}/\text{Al} = 37.5$) or FAU ($\text{Si}/\text{Al} = 40$) are incorporated into the MFI crystals. BEA and FAU transformations to MFI required 24–40 h (Table 1), while direct hydrothermal syntheses of MFI starting from Si and Al sources typically require 2–15 days with or without SDA.³³ Thus, the presence of a common CBU between parent and product zeolites or in the absence of it, product seeds in the synthesis assist the nucleation of MFI crystals and do so more effectively from intermediates formed from parent zeolites than from amorphous silica and alumina gels, resulting in significantly shorter synthesis times. As a result, such protocols may provide alternate routes to the synthesis of some zeolites; such routes may shorten crystallization times and decrease the cost and environmental impact associated with organic moieties.

Next, we show how such interzeolite transformations can be used to encapsulate metal clusters within MFI via interzeolite transformations of BEA and FAU zeolites containing encapsulated clusters as the parent materials. We first provide

evidence for the encapsulation of metal clusters within these parent zeolites, which are then transformed to MFI with retention of encapsulated clusters.

3.1. Encapsulation of Metal Clusters within BEA and FAU Parent Zeolites via Aqueous Exchange Methods.

3.1.1. Assessment of Cluster Size and Uniformity in BEA and FAU Parent Zeolites. This section describes the synthesis, structural characterization, and catalytic properties of Pt, Ru and Rh clusters within BEA and FAU parent zeolites, with the intent to use these materials for subsequent conversion to MFI. BEA and FAU containing metals (M/BEA and M/FAU, respectively; M = Pt, Ru, Rh) were synthesized via ion-exchange with Pt, Rh, and Ru precursors in aqueous solutions of $[\text{Pt}(\text{NH}_3)_4](\text{NO}_3)_2$, $[\text{Ru}(\text{NH}_3)_6]\text{Cl}_3$ or $[\text{Rh}(\text{NH}_2\text{CH}_2\text{CH}_2\text{NH}_2)_3]\text{Cl}_3 \cdot 3\text{H}_2\text{O}$ at 353 K (using the procedures described in subsection 2.2.3).

TEM images of Pt clusters dispersed on BEA and FAU zeolites after exchange and thermal treatment in flowing air at 623 K for 3 h and in H_2 at 573 K for 2 h are shown in Figure 2. These images show the presence of small Pt clusters in BEA ($d_{\text{TEM}} = 1.6 \text{ nm}$; Table 2, calculated using eq 2) and FAU ($d_{\text{TEM}} = 1.7 \text{ nm}$; Table 2); these clusters are narrowly distributed in size (DI = 1.07 and 1.03 for BEA and FAU, respectively; Table 2, from eq 3) and reside throughout zeolite crystals. Chemisorptive titrations of metal surfaces with H_2 gave Pt fractional dispersions of 0.88 for Pt/BEA and 0.78 for Pt/FAU (Table 2); these values correspond to mean cluster diameters (d_{chem}) of 1.3 and 1.4 nm, respectively, when clusters are

Table 2. Metal Loadings, Dispersions, Mean Sizes, and Dispersity of Metal Clusters Dispersed on SiO_2 , BEA, FAU, and MFI

| sample | metal loading (% wt) ^a | D^b | d_{chem}^c (nm) ^c | d_{TEM}^d (nm) | dispersity index (DI) |
|---------------------|--------------------------------------|-------|--|----------------------------|--------------------------|
| Pt/ SiO_2 | 0.79 | 0.61 | 1.8 | 2.4 | 1.96 |
| Ru/ SiO_2 | 0.51 | 0.22 | 3.7 | 4.8 | |
| Rh/ SiO_2 | 1.10 | 0.60 | 1.8 | 2.1 | |
| Pt/BEA | 0.85 | 0.88 | 1.3 | 1.6 | 1.07 |
| Ru/BEA | 0.64 | 0.63 | 1.4 | 1.4 | 1.08 |
| Pt/FAU | 1.23 | 0.78 | 1.4 | 1.7 | 1.03 |
| Ru/FAU | 0.95 | 0.59 | 1.5 | 1.7 | 1.16 |
| Rh/FAU | 0.80 | 0.85 | 1.3 | 1.5 | 1.09 |
| Pt/MFI _B | 1.01 | 0.80 | 1.4 | 1.7 | 1.41 |
| Ru/MFI _B | 1.23 | 0.70 | 1.2 | 1.3 | 1.16 |
| Pt/MFI _F | 1.23 | 0.75 | 1.5 | 1.0 | 1.09 |
| Ru/MFI _F | 1.33 | 0.72 | 1.2 | 1.5 | 1.16 |
| Rh/MFI _F | 1.55 | 0.96 | 1.1 | 1.5 | 1.09 |

^aAnalyzed by inductively coupled plasma optical emission spectroscopy. ^bMetal dispersion estimated from H_2 chemisorptions. ^cMean cluster diameter estimated from the metal dispersion obtained from H_2 chemisorption measurements.²³ ^dSurface-area-weighted mean cluster diameter (d_{TEM}) estimated from TEM analysis, $d_{\text{TEM}} = \sum n_i d_i^3 / \sum n_i d_i^2$ ²⁵, the mean cluster diameters of metal supported on SiO_2 samples are quoted from ref 16.

spherical and have the bulk density of Pt metal.²³ In contrast, Pt clusters at similar loading and prepared by incipient wetness impregnation of mesoporous SiO_2 with same metal precursor are larger ($d_{\text{TEM}} = 2.4$ nm, $d_{\text{chem}} = 1.8$ nm; Table 2) and more broadly distributed (DI = 1.96; Table 2) than in Pt/BEA and Pt/FAU samples, suggesting that confinement within small zeolite voids inhibits sintering and the concomitant broadening of the cluster size distribution. The chemisorption-derived Pt cluster diameters (1.3–1.4 nm) in these zeolitic samples agree well with those measured by TEM (1.6–1.7 nm), indicating that the clusters detectable by microscopy contain clean surfaces accessible for chemisorption by H_2 titrants and that the ligands present during synthesis were completely removed by the thermal treatments used. Similarly, Ru clusters dispersed in BEA, and Ru and Rh clusters in FAU show d_{TEM} values of 1.4, 1.7, and 1.5 nm, DI values of 1.08, 1.16, and 1.09, and d_{chem} values of 1.4, 1.5, and 1.3 nm, respectively; consistent with the presence of small, uniform and clean metal clusters dispersed throughout the BEA and FAU parent zeolites.

3.1.2. Catalytic Evidence for Encapsulation of Metal Clusters in BEA and FAU Parent Zeolites. The small apertures in zeolites allow them to sieve reactants and products based on

their molecular size. The relative reaction rates for small and large reactants at sites residing within accessible and inaccessible locations can be used to assess the fraction of the metal surface area that resides within zeolite voids. The rates of hydrogenation of toluene and 1,3,5-TIPB reactants (0.59²⁶ and 0.84 nm²⁷ respective kinetic diameters) were used to confirm the predominant presence of metal (Pt, Ru, Rh) clusters within the parent BEA (~0.70 nm aperture) and FAU (0.74 nm aperture) materials. Toluene, but not 1,3,5-TIPB, can access active metal sites encapsulated within BEA and FAU voids via diffusion through their interconnected voids and apertures.²⁷

Encapsulation selectivities were determined by first measuring the rates of hydrogenation of small (toluene) and large (1,3,5-TIPB) reactants on unconstrained clusters dispersed on SiO_2 ($\chi_{\text{SiO}_2} = r_{\text{toluene}}/r_{1,3,5\text{-TIPB}}$); this rate ratio reflects the relative reactivity of these two reactant molecules in the absence of diffusional constraints. A similar measurement of this ratio on metal-zeolite samples (χ_{zeolite}) can then be used to determine the encapsulation selectivity parameter ($\phi = \chi_{\text{zeolite}}/\chi_{\text{SiO}_2}$), which reflects the ratio of the surface area of all the clusters in the sample to that of clusters at (fully accessible) locations outside zeolite crystals. The encapsulation selectivity is therefore a rigorous indicator of the extent to which the active surfaces are contained within microporous networks, which toluene (but not 1,3,5-TIPB) can access. This encapsulation selectivity parameter approaches unity for clusters with unimpeded access to reactants, such as those at external zeolite surfaces. Values of ϕ much larger than unity (~10, indicating >90% of the active metal surfaces reside within zeolitic voids), in contrast, provide evidence that metal clusters predominantly reside within regions that restrict access to the large reactants and, therefore, are taken here as evidence of successful encapsulation.

Toluene and 1,3,5-TIPB hydrogenation reactions led to the respective exclusive formation of methyl cyclohexane and (*cis*- and *trans*)-1,3,5-triisopropyl cyclohexane on all samples. Table 3 shows arene hydrogenation turnover rates on Pt, Ru, and Rh clusters dispersed on BEA (M/BEA), FAU (M/FAU), and SiO_2 (M/ SiO_2). Toluene hydrogenation turnover rates were very similar on Pt/BEA and Pt/FAU than on Pt/ SiO_2 (Table 3), consistent with the absence of cluster size effects or diffusional constraints for toluene reactions. In contrast, 1,3,5-TIPB turnover rates were much lower on Pt/BEA and Pt/FAU than on Pt/ SiO_2 (by factors of 44 and 38, respectively, Table 3), indicating that 1,3,5-TIPB cannot access most of the clusters in BEA and FAU samples. The ratios of toluene to 1,3,5-TIPB hydrogenation turnover rates were therefore much higher on Pt/BEA and Pt/FAU (by factors of 180 and 160, respectively)

Table 3. Catalytic Properties of Metal Containing BEA, FAU, and SiO_2 Samples in Hydrogenation of Arenes^a

| sample | r_{toluene} (mol $(\text{mol}_{\text{surf-metal}}^{-1} \text{s}^{-1})^b$) | $r_{1,3,5\text{-TIPB}}$ (mol $(\text{mol}_{\text{surf-metal}}^{-1} \text{s}^{-1})^b$) | χ_j ($j = \text{zeolite, SiO}_2$) ^c | ϕ^d |
|--------------------|---|--|---|----------|
| Pt/BEA | 1.26 | 0.007 | 180.0 | 40.9 |
| Pt/FAU | 1.28 | 0.008 | 160.0 | 36.4 |
| Pt/ SiO_2 | 1.35 | 0.306 | 4.4 | 1.0 |
| Ru/BEA | 0.112 | 0.001 | 112.0 | 14.3 |
| Ru/FAU | 0.120 | 0.001 | 120.0 | 15.4 |
| Ru/ SiO_2 | 0.173 | 0.022 | 7.8 | 1.0 |
| Rh/FAU | 0.019 | 0.0003 | 63.3 | 21.8 |
| Rh/ SiO_2 | 0.023 | 0.008 | 2.9 | 1.0 |

^aHydrogenations were carried out with 0.35 kPa toluene/0.15 kPa 1,3,5-TIPB and 100 kPa H_2 at 473 K. ^bReaction turnover rate is defined as mole of reactant converted per mole of surface metal atoms per second. ^c $\chi_j = r_{\text{toluene}}/r_{1,3,5\text{-TIPB}}$; $j = \text{zeolite, SiO}_2$. ^d $\phi = \chi_{\text{zeolite}}/\chi_{\text{SiO}_2}$.

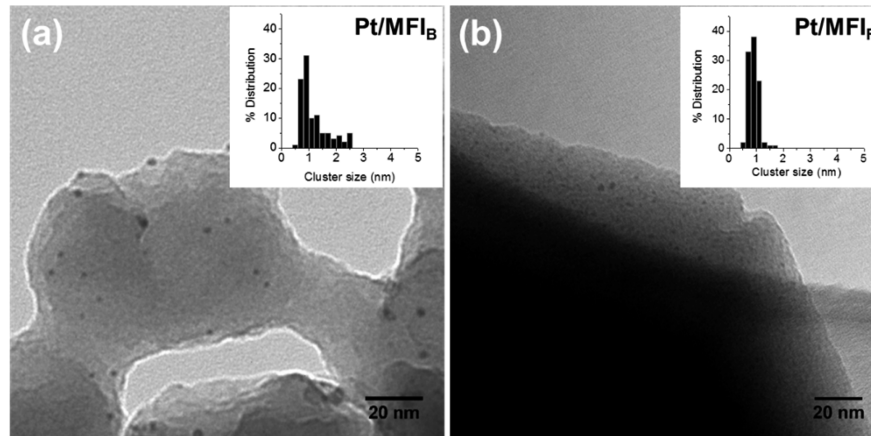


Figure 3. TEM images and metal cluster size distributions of Pt containing MFI samples synthesized by interzeolite transformations of (a) BEA and (b) FAU zeolites containing Pt clusters as parent materials.

than on Pt/SiO_2 (4.4), resulting in encapsulation selectivity parameters (ϕ) of 40.9 and 36.4 for Pt/BEA and Pt/FAU , respectively (Table 3). Encapsulation selectivity parameters (Table 3) were 14.3 and 15.4 for Ru clusters in BEA and FAU parent zeolites, respectively, and 21.8 for Rh clusters in FAU samples. These large encapsulation selectivity values confirm that clusters of all these metals reside preferentially within the void structures of BEA or FAU zeolites when such samples are prepared using ion exchange and reduction procedures reported here. These materials are therefore well-suited to assess whether encapsulated metal clusters can (i) interfere with FAU or BEA transformations to MFI and/or (ii) be retained during interzeolite transformations.

3.2. MFI-Encapsulated Metal Clusters via Interzeolite Transformations of BEA and FAU. **3.2.1. Assessment of the Size and Uniformity of Metal Clusters in MFI.** M/BEA and M/FAU (M = Pt, Ru, Rh) zeolites containing metal clusters (subsection 2.2.3) are used here as precursor materials to form MFI using the hydrothermal protocols described in subsections 2.2.4 and 2.2.5, and shown to be successful in the absence of metal clusters (section 3). The resulting samples are denoted here as M/MFI_B (derived from M/BEA) and M/MFI_F (derived from M/FAU). Neither seeds nor SDA were used in M/BEA to M/MFI transformations; MFI seeds were used (instead of SDA) in M/FAU to M/MFI transformations so as to avoid electrostatic and van der Waals interactions that may cause SDA species to dislodge clusters from intracrystalline MFI voids during hydrothermal interconversion protocols.¹⁴

BEA and FAU zeolites were successfully transformed into MFI with or without encapsulated clusters in the parent zeolites (X-ray diffractograms; without metals, Figure 1; with metals, Figure S1). Subsequent treatments in flowing air at 673 K for 3 h and then in flowing H_2 at 623 K for 2 h did not cause detectable changes in MFI crystallinity. X-Ray diffractograms also did not show any lines for metal or oxide phases in M/MFI (M = Pt, Ru, Rh; Figure S1) after H_2 treatment at 623 K for 2 h (1.01–1.55% wt metal; Table 2), consistent with the absence of large metal crystallites in MFI daughter structures.

TEM images of reduced and passivated M/MFI samples (M = Pt, Ru, Rh) detected small clusters uniform in size (Pt/MFI_B and Pt/MFI_F in Figure 3, Ru/MFI_B , Ru/MFI_F , and Rh/MFI_F in Figure S2). The surface-averaged mean cluster diameters and DI values obtained from TEM measurements (Table 2) were 1.7 nm and 1.41 for Pt/MFI_B (vs 1.6 nm and 1.07 in parent Pt/FAU and 1.0 nm and 1.09 for Pt/MFI_F (vs 1.7 nm and 1.03 in parent Pt/FAU).

The DI values of parent zeolites were only slightly larger than the corresponding product zeolites, suggesting that significant sintering or coalescence did not occur during interzeolite transformations. H_2 chemisorption measurements on Pt/MFI gave an average cluster diameter of 1.4 when it was prepared from Pt/BEA ($d_{\text{chem}} = 1.3$) and 1.5 when synthesized from Pt/FAU ($d_{\text{chem}} = 1.4$). These chemisorption-derived mean cluster diameters agree well with surface-averaged cluster diameters from TEM (1.0–1.7; Table 2), suggesting the absence of residues deposited from synthesis mixtures and not removed during post-synthesis treatments. The sizes of these metal clusters, however, are larger than the intersection voids of MFI (0.64 nm included sphere diameter²⁸), which reflect the local disruption of the crystal structures near the location of the clusters. These locations represent only 0.4–0.5% of the void volume; as a result, they are not detectable in diffractograms and do not disrupt the ability of the void structure to sieve molecules based on size over the relevant distance for diffusion (crystal diameter). In contrast, Pt/SiO_2 showed a d_{TEM} value of 2.4 nm, a d_{chem} value of 1.8 nm, and a DI value of 1.96; these sizes and dispersities are significantly larger than those for the clusters dispersed on parent (Pt/BEA and Pt/FAU) and product (Pt/MFI) zeolite samples, suggesting that confining environments are essential for the synthesis of small and uniform metal clusters.

Similarly, DI values (1.09–1.16 (vs 1.08–1.16 for parent zeolites); Table 2), TEM-derived surface-averaged cluster diameters (1.3–1.5 (vs 1.4–1.7 for parent zeolites); Table 2), and chemisorption-derived mean cluster diameters (1.1–1.2 (vs 1.3–1.5 for parent zeolites); Table 2) for Ru/MFI_B , Ru/MFI_F , and Rh/MFI_F were also consistent with the presence of small, uniform, and clean metal clusters within MFI voids and with the retention of encapsulation during transformations from parent BEA or FAU materials.

3.2.2. Assessment of Encapsulation Selectivity of MFI-Encapsulated Metal Clusters from Selective Hydrogenation of Arenes. Hydrogenation rates of toluene and 1,3,5-TMB (0.59 and 0.74 nm kinetic diameters) were used to assess the extent of confinement of Pt, Ru, and Rh clusters within product MFI zeolites (~0.55 nm apertures). Toluene (but not 1,3,5-TMB) can access active sites encapsulated within MFI voids via diffusion through their interconnected voids and apertures.³⁴

Table 4. Catalytic Properties of Metal Containing MFI and SiO₂ Samples in Hydrogenation of Arenes^a

| sample | r_{toluene} (mol (mol _{surf-metal} ⁻¹ s ⁻¹)) ^b | $r_{1,3,5\text{-TMB}}$ (mol (mol _{surf-metal} ⁻¹ s ⁻¹)) ^b | χ_j ($j = \text{MFI}, \text{SiO}_2$) ^c | ϕ^d |
|---------------------|--|--|--|----------|
| Pt/MFI _B | 1.12 | 0.05 | 22.4 | 8.3 |
| Pt/MFI _F | 0.50 | 0.01 | 50.0 | 18.5 |
| Pt/SiO ₂ | 1.35 | 0.50 | 2.7 | 1.0 |
| Ru/MFI _B | 0.015 | 0.0001 | 150.0 | 22.7 |
| Ru/MFI _F | 0.012 | 0.0002 | 60.0 | 9.1 |
| Ru/SiO ₂ | 0.173 | 0.0260 | 6.6 | 1.0 |
| Rh/MFI _F | 0.017 | 0.001 | 17.0 | 8.1 |
| Rh/SiO ₂ | 0.023 | 0.011 | 2.1 | 1.0 |

^aHydrogenations were carried out with 0.35 kPa toluene/0.26 kPa 1,3,5-TMB and 100 kPa H₂ at 473 K. ^bReaction turnover rate is defined as moles of reactant converted per mole of surface metal atoms per second. ^c $\chi_j = r_{\text{toluene}}/r_{1,3,5\text{-TMB}}$, $j = \text{MFI}, \text{SiO}_2$. ^d $\phi = \chi_{\text{MFI}}/\chi_{\text{SiO}_2}$.

1,3,5-TMB hydrogenation reaction led to the exclusive formation of (*cis*- and *trans*)-1,3,5-trimethyl cyclohexane on all catalysts. Table 4 shows turnover rates for the hydrogenation of these arenes on metal clusters (M = Pt, Ru, Rh) dispersed on SiO₂ (M/SiO₂) and on MFI (M/MFI_B and M/MFI_F). Toluene hydrogenation turnover rates were somewhat lower on Pt/MFI_B and Pt/MFI_F than on Pt/SiO₂ samples (by factors of 1.2 and 2.7, respectively, Table 4), possibly because access to metal clusters was restricted by diffusion through the MFI apertures (~0.55 nm), which are similar to the size of toluene (0.59 nm kinetic diameter²⁶) or due to the partial blockage of the pore entrances by the impervious debris or amorphous solids, present in small amount in these materials (textural characterization, Table S1). In contrast, 1,3,5-TMB turnover rates were much smaller on Pt/MFI_B and Pt/MFI_F than on Pt/SiO₂ samples (by factors of 10 and 50, respectively, Table 4), suggesting that most of the active surfaces reside within MFI voids inaccessible to 1,3,5-TMB. Pt/MFI_B and Pt/MFI_F, synthesized via interzeolite transformations of Pt/BEA and Pt/FAU, respectively, gave much higher χ values (22.4 and 50.0 for Pt/MFI_B and Pt/MFI_F, respectively) for selective hydrogenation of toluene and 1,3,5-TMB than for the Pt clusters dispersed on SiO₂ ($\chi_{\text{SiO}_2} = 2.7$; Table 4); these values lead, in turn, to high encapsulation selectivities ($\phi = 8.3$ and 18.5, respectively; Table 4), consistent with the preferential encapsulation of Pt clusters within MFI voids. The encapsulation selectivity value was 8.3 for Pt/MFI_B (vs 40.9 for Pt/BEA) and 18.5 for Pt/MFI_F (vs 36.4 for Pt/FAU); these encapsulation selectivities for product zeolites are lower than the values of their respective parent zeolite, consistent with the retention of most of the clusters within zeolitic pores during transformations, and consistent with slight increase in DI values from parent to product zeolites. Ru/MFI_B, Ru/MFI_F and Rh/MFI_F synthesized also gave much larger χ values (150, 60 and 17, respectively; Table 4) than for the respective metals dispersed on SiO₂ (6.6 and 2.1 for Ru and Rh, respectively; Table 4) and consequently, high encapsulation selectivities for hydrogenation reactions (22.7, 9.1 and 8.1, respectively (vs 14.3, 15.4, 21.8 for their corresponding parent zeolite); Table 4), indicating that Ru and Rh clusters on these zeolite samples indeed reside predominantly within locations accessible only to the smaller toluene reactant and that the encapsulation of these clusters within zeolitic voids was preserved during interzeolite transformations.

The high encapsulation selectivity values (8–23; Table 4) for M/MFI samples also indicate that for all these samples more than 88% of the metal surface areas are contained within locations accessible to toluene but not to 1,3,5-TMB. These data, taken together with the TEM- and chemisorption-derived

mean cluster diameters and size uniformity, suggest that most of the metal clusters initially present within BEA or FAU voids remained inside the zeolitic pores during the transformations, retaining encapsulation in the resulting MFI samples, that can select reactant based on molecular size and allow access to active sites only by the reactants smaller than the MFI aperture sizes.

Next, we address the challenges of direct hydrothermal crystallization approaches for encapsulation within MFI, which can be circumvented, as we have shown in this section, using interzeolite transformation protocols.

3.3. Synthesis of MFI-Encapsulated Metal Clusters and Identification and Control of Key Parameters That Affect Encapsulation. The successful synthesis of encapsulated clusters requires that MFI nucleation and growth from basic media occur before insoluble colloidal hydroxides form via reactions of metal precursors with OH⁻ species at the high pH required for synthesis. We seek here synthesis conditions that promote nucleation and growth, while inhibiting the premature precipitation of metal precursors. A schematic depiction of how synthesis strategies and conditions may accomplish such objectives is shown in Figure 4. In what follows, we examine these synthesis parameters according to the regions depicted in Figure 4 (e.g., whether OH⁻ or F⁻ are used as the mineralizing agents) with the objective of controlling the relative rates of

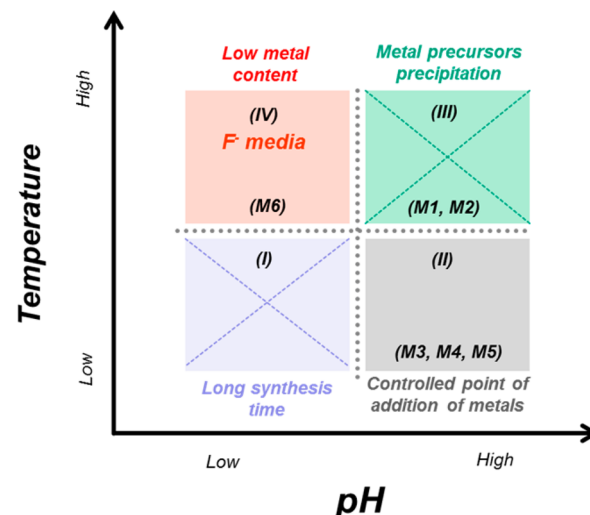


Figure 4. Schematic representation of the synthesis factors that limit encapsulation of metal clusters within MFI over a broad range of synthesis conditions. Mi represents the synthesis method used (Table 5).

Table 5. Synthesis Procedures and Encapsulation Selectivities for Metal-Containing MFI Synthesized by Direct Hydrothermal Syntheses

| name | sample | composition | metal precursor (composition) ^a | T (K) | t (d) ^b | preparation method | Φ^c | comments |
|------|--------|---|--|-------|--------------------|--|----------|---|
| M1 | Ru/MFI | 70 SiO ₂ : 1.0 Al ₂ O ₃ : 11.5 Na ₂ O: 2800 H ₂ O | RuCl ₃ (1.9) | 433 | 3 | direct hydrothermal synthesis with added RuCl ₃ | 0.95 | metal precursor decomposed in the synthesis |
| M2 | Pt/MFI | 70 SiO ₂ : 1.0 Al ₂ O ₃ : 11.5 Na ₂ O: 2800 H ₂ O | Pt(NH ₃) ₄ (NO ₃) ₂ (3.5) | 433 | 3 | direct hydrothermal synthesis with ligand-stabilized metal precursor | 0.98 | metal precursor decomposed in the synthesis |
| M3 | Pt/MFI | 0.04 TPABr: 0.003 Al ₂ O ₃ : 1 SiO ₂ : 120 H ₂ O: 0.322 OH ⁻ | Pt(NH ₃) ₄ (NO ₃) ₂ (0.05) | 383 | 12 | low T synthesis with excess amount of template | 0.85 | competition between metal precursor and SDA |
| M4 | Pt/MFI | 0.02 TPABr: 0.003 Al ₂ O ₃ : 1 SiO ₂ : 120 H ₂ O: 0.322 OH ⁻ | Pt(NH ₃) ₄ (NO ₃) ₂ (0.05) | 383 | 15 | low T synthesis with substoichiometric amount of template | 0.90 | poor crystallization of resulted MFI, metal precursor precipitation |
| M5 | Pt/MFI | 0.03 TPABr: 0.003 Al ₂ O ₃ : 1 SiO ₂ : 120 H ₂ O: 0.322 OH ⁻ | Pt(NH ₃) ₄ (NO ₃) ₂ (0.05) | 383 | 15 | metal precursor added after 5 days of synthesis | 5 | successful encapsulation |
| M6 | Pt/MFI | 0.07 TPABr: 1.0 TEOS: 0.012 NaAlO ₂ : 1.2 NH ₄ F: 80 H ₂ O | Pt(NH ₃) ₄ (NO ₃) ₂ (0.05) | 443 | 7 | high T, low pH synthesis in fluoride media | 12 | successful encapsulation, low metal loading |

^aThe molar compositions of metal precursors are reported relative to SiO₂. ^bt = time required for synthesis in days. ^c $\phi = \chi_{\text{MFI}}/\chi_{\text{SiO}_2}$, $\chi_j = r_{\text{toluene}}/r_{1,3,5\text{-TMB}}$; j = MFI, SiO₂.

zeolite nucleation and precursor precipitation. Additional details of the synthesis conditions used are given in Table 5, together with the encapsulation selectivity values of the catalytic materials formed. The encapsulation selectivity for these metal-zeolite materials are reported from the rates of hydrogenation of toluene and 1,3,5-TMB, as done for the materials prepared by interzeolite transformations of BEA or FAU into MFI.

In region III (Figure 4), the synthesis was carried out at high pH and temperature (pH 12, 433 K), which favors fast nucleation and crystallization of MFI, but also the rapid formation of insoluble hydroxides from the metal precursors. The encapsulation selectivity parameter values for the products formed at these conditions was near unity (0.95 for Ru using RuCl₃ precursor; M1 and 0.98 for Pt using Pt(NH₃)₄(NO₃)₂ precursor; M2, Table 5), suggesting the prevalence of external zeolitic clusters. The use of SDA moieties (tetrapropylammonium bromide) also promotes rapid and selective MFI crystallization, but such species can fill the intracrystalline voids, thus preventing the encapsulation of the metal precursors, even as solvated monomers. The selectivity parameter for the product in this case was, again, near unity (0.85 for Pt using Pt(NH₃)₄(NO₃)₂ precursor; M3, Table 5), indicating that the clusters formed do not reside during intracrystalline MFI voids. As a result, the use of SDA species must be avoided (or their concentration kept very low) during synthesis, while also maintaining conditions that disfavor the formation of colloidal hydroxides of metal precursors. Using the minimal amount of SDA required to fill the intracrystalline voids, while keeping low temperatures (383 K) but high OH⁻ levels (pH 12.9), did not lead to crystallization of MFI structures (M4, Table 5) and the amorphous solids formed did not provide any access constraints (0.90 encapsulation selectivity; Table 5).

These findings led us to consider the introduction of the metal precursors after hydrothermal treatments of the alumina and silica precursors at conditions (region II; Figure 4) but before the nucleation of MFI, which formed only after several days (M5, Table 5), with the aim to limit the time that metal precursors were subjected to conditions conducive to precipitation. During the initial period of hydrothermal treatments, MFI nuclei form slowly and crystals then grow much more rapidly,^{35,36} and often require milder conditions of temperature or pH. These experiments (M5, Table 5) involved

the treatment of the starting aluminosilicate gel (Si/Al = 166) at 383 K and pH 12.9 for 5 days, after which the autoclave contents were briefly cooled to ambient temperature and a solution of the metal complex (Pt(NH₃)₄(NO₃)₂, Pt precursor/SiO₂ = 0.05) was added to the contents of the autoclave. This autoclave was sealed again, heated to 383 K, and held at this temperature for 10 days (X-ray diffraction patterns, Figure S3). The Pt encapsulation selectivity parameter for this sample was 5.0 (Table 5), compared to the much smaller values for the synthesis protocols described earlier in this section (0.85–0.98; M1–M4, Table 5). The modest encapsulation selectivity in this case indicates that Pt clusters were preferentially encapsulated within MFI voids. This encapsulation selectivity value, however, is much smaller than that achieved by interzeolite transformation protocols (8–23; Table 4), where the large pore zeolites containing metal clusters were converted to MFI, while retaining the encapsulation.

Lower temperatures and OH⁻ concentrations, as well as the substitution of OH⁻ with F⁻, were also explored. At the low temperature and pH of region I (403–523 K, 7–11, Figure 4), metal precursors are stable but so are the silicate species that assemble into MFI frameworks, causing synthesis times, in this case, to be very long, in some reported cases on the order of several months.³⁷

Region IV (Figure 4) involves the use of fluoride instead of hydroxide anions, which leads to MFI synthesis mixtures at near neutral pH conditions;²² these conditions are likely to preserve metal precursors in solution throughout hydrothermal crystallization of MFI structures. Indeed, such synthesis protocols (M6, Table 5; 443 K, pH 7), in the presence of Pt(NH₃)₄(NO₃)₂ precursors (Pt precursor/SiO₂ = 0.05, Table 5), led to an even higher encapsulation selectivity parameter ($\phi = 12$; Table 5) than the delayed introduction protocols described in the previous paragraph. The fraction of the metal in the synthesis mixture that was retained in the solids products (0.08), however, was very small, leading to Pt contents below 0.1% wt (from ICP analysis) in the final Pt/MFI sample. We conclude that the neutral pH conditions allowed by the use of F⁻ anions prevented the precipitation of metal precursors as hydroxides, but also appeared to cause the replacement of the ligands in the solvated precursors with F⁻ anions, possibly leading to the formation of neutral or anionic complexes that resisted occlusion within MFI nuclei as they incipiently formed.

Thus, encapsulation was achieved via direct hydrothermal synthesis protocols by introducing metal precursors later in the zeolite synthesis or by decreasing the pH using F^- instead of OH^- as mineralizing agents. These methods led to modest encapsulation selectivities ($\phi = 5\text{--}12$; Table 5) using delayed precursor addition and direct hydrothermal synthesis in fluoride media and to low encapsulation yields (Pt contents < 0.1% wt) using fluoride synthesis. Interzeolite transformation protocols, in contrast, circumvent the encapsulation challenges in direct hydrothermal syntheses and, in doing so, provide a general method for the encapsulation of metal clusters within the voids of MFI crystals with high selectivities ($\phi = 8\text{--}23$; Table 4) and metal contents (1.01–1.55% wt; Table 2); such protocols merely require that such cations be able to exchange into a parent zeolite with voids larger than MFI and exhibiting a lower framework density (here BEA or FAU), which can be subsequently converted into a daughter zeolite (here MFI), for which exchange or more direct methods of encapsulation are not feasible. It seems reasonable to infer that such interzeolite transformation approaches for the containment of metal clusters can be generally extended to any metals with cationic complexes in aqueous media and to any interconversions that increase zeolite framework density, whether they occur spontaneously or through the use of kinetic aids (e.g., seeds or organic structure-directing agents) under hydrothermal conditions.

4. CONCLUSION

Successful encapsulation of metal clusters (Pt, Ru, Rh) within MFI voids was achieved via interzeolite transformations of metal containing BEA or FAU zeolites, by low temperature hydrothermal synthesis with controlled point of addition of metal precursors, and direct hydrothermal synthesis in fluoride media. Interzeolite transformations provide an opportunity to synthesize zeolites with less time and cost, and represent a more economical and environmentally conscious approach, compared to direct hydrothermal synthesis methods, and do so by assisting the nucleation of the desired product zeolite and avoiding the use of organic structure directing agents during synthesis. These interzeolite transformation methods also led to the successful encapsulation of metal clusters within MFI zeolites, where encapsulation was not otherwise feasible by developed protocols involving direct hydrothermal synthesis with ligand-stabilized metal precursors and post-synthesis exchange. X-ray diffraction, electron microscopy, and H_2 chemisorption measurements, when combined, confirmed the transformation of parent zeolites to MFI and the presence of small, uniform, and clean metal clusters. The relative rates of hydrogenation of toluene and 1,3,5-TMB on metal clusters dispersed on MFI and SiO_2 showed that the metal clusters in the zeolitic samples reside predominately within MFI voids, where they were accessible only to the smaller toluene reactant. We expect that the developed interzeolite transformation approach for the synthesis of MFI with/without encapsulated metal clusters can be extended further to zeolites of different frameworks, void environments, and framework compositions and to encapsulate clusters of other metals, metal oxides, and metal sulfides of catalytic importance.

■ ASSOCIATED CONTENT

S Supporting Information

X-Ray diffraction patterns of M/MFI samples (M = Pt, Ru, Rh) and TEM images of M/MFI (M = Ru, Rh) samples synthesized

via interzeolite transformations, X-ray diffraction patterns of Pt/MFI sample synthesized by direct hydrothermal synthesis (M5, Table 5), and textural properties of Pt/MFI_B and Pt/MFI_F samples. This material is available free of charge via the Internet at <http://pubs.acs.org>.

■ AUTHOR INFORMATION

Corresponding Authors

iglesia@berkeley.edu
sizo@chevron.com

Present Address

[†]S.I.Z.: Chevron Energy Technology Company, Richmond, California 94804, USA.

Notes

The authors declare the following competing financial interest(s): (1) The funding for the research came from Chevron Energy and Technology Co. (2) Stacey I. Zones is an employee of this company and then more generally also a stockholder in Chevron Corp.

■ ACKNOWLEDGMENTS

We thank Reena Zalpuri (Electron Microscope Lab) for help with the TEM instrument, Edwin Yik and Dr. Xueyi Zhang for the careful review of this manuscript, and Chevron Energy Technology Company for the financial support for this research.

■ REFERENCES

- (1) Csicsery, S. M. *Zeolites* **1984**, *4*, 202.
- (2) Weisz, P. B.; Frilette, V. J.; Maatman, R. W.; Mower, E. B. *J. Catal.* **1962**, *1*, 307.
- (3) Davis, M. E.; Lobo, R. F. *Chem. Mater.* **1992**, *4*, 756.
- (4) Davis, M. E. *Chem. Mater.* **2014**, *26*, 239–245.
- (5) Bhan, A.; Tsapatsis, M. *Curr. Opin. Chem. Eng.* **2013**, *2*, 320–324.
- (6) Moliner, M.; Martínez, C.; Corma, A. *Chem. Mater.* **2014**, *26*, 246–258.
- (7) Gates, B. C. *Chem. Rev.* **1995**, *95*, 511.
- (8) Flytzani-Stephanopoulos, M.; Gates, B. C. *Annu. Rev. Chem. Biomol. Eng.* **2012**, *3*, 545.
- (9) Wu, J. C. S.; Goodwin, J. G., Jr.; Davis, M. J. *Catal.* **1990**, *125*, 488.
- (10) Gallezot, P. *Post-Synthesis Modification I* **2002**, 257.
- (11) Sachtler, W. M. H. *Acc. Chem. Res.* **1993**, *26*, 383.
- (12) Guczi, L.; Kiricsi, I. *Appl. Catal., A* **1999**, *186*, 375.
- (13) Zhan, B.-Z.; White, M. A.; Sham, T. K.; Pincock, J. A.; Doucet, R. J.; Rao, K. V. R.; Robertson, K. N.; Cameron, T. S. *J. Am. Chem. Soc.* **2003**, *125*, 2195.
- (14) Altwasser, S.; Gläser, R.; Lo, A. S.; Liu, P.-H.; Chao, K.-J.; Weitkamp, J. *Microporous Mesoporous Mater.* **2006**, *89*, 109.
- (15) Zhan, B.-Z.; Iglesia, E. *Angew. Chem., Int. Ed.* **2007**, *46*, 3697–3700.
- (16) Choi, M.; Wu, Z.; Iglesia, E. *J. Am. Chem. Soc.* **2010**, *132*, 9129.
- (17) Wu, Z.; Goel, S.; Choi, M.; Iglesia, E. *J. Catal.* **2014**, *311*, 458–468.
- (18) Goel, S.; Wu, Z.; Zones, S. I.; Iglesia, E. *J. Am. Chem. Soc.* **2012**, *134*, 17688.
- (19) Zones, S. I. *J. Chem. Soc., Faraday Trans.* **1991**, *87*, 3709.
- (20) Sano, T.; Itakura, M.; Sadakane, M. *J. Japan Petro. Inst.* **2013**, *56*, 183–197.
- (21) Kiyozumi, Y.; Suzuki, K.; Shin, S.; Okado, H.; Noguchi, K. US4579994 A, April 1, 1986.
- (22) Louis, B.; Kiwi-Minsker, L. *Microporous Mesoporous Mater.* **2004**, *74*, 171.
- (23) Bergeret, G.; Gallezot, P. *Handbook of Heterogeneous Catalysis*; Wiley-VCH Verlag GmbH & Co. KgaA: New York, 2008.

- (24) Stepto, R. F. T. *Pure Appl. Chem.* **2009**, *81*, 351.
- (25) Schneider, M.; Duff, D.; Mallat, T.; Wildberger, M.; Baiker, A. J. *Catal.* **1994**, *147*, 500.
- (26) Somiya, S., Ed. *Handbook of Advanced Ceramics: Materials, Applications, Processing, and Properties*; Academic Press: Waltham, MA, 2013.
- (27) Caro, J.; Noack, M. In *Advances in Nanoporous Materials*; Ernst, S., Ed.; Elsevier: New York, 2010; Vol. 1, pp 1–96.
- (28) Baerlocher, C.; McCusker, L. B. Database of Zeolite Structures: <http://www.iza-structure.org/databases/>.
- (29) Maldonado, M.; Oleksiak, M. D.; Chinta, S.; Rimer, J. D. *J. Am. Chem. Soc.* **2013**, *135*, 2641.
- (30) Itabashi, K.; Kamimura, Y.; Iyoki, K.; Shimojima, A.; Okubo, T. *A. J. Am. Chem. Soc.* **2012**, *134*, 11542.
- (31) Iyoki, K.; Itabashi, K.; Okubo, T. *Microporous Mesoporous Mater.* **2014**, *189*, 22.
- (32) Xie, B.; Song, J.; Ren, L.; Ji, Y.; Li, J.; Xiao, F.-S. *Chem. Mater.* **2008**, *20*, 4533–4535.
- (33) Moore, R. M.; Katzer, J. R. *AIChE J.* **1972**, *18*, 816.
- (34) Davis, T. M.; Drews, T. O.; Ramanan, H.; He, C.; Dong, J.; Schnablegger, H.; Katsoulakis, M. A.; Kokkoli, E.; McCormick, A. V.; Penn, R. L.; Tsapatsis, M. *Nat. Mater.* **2006**, *5*, 400–408.
- (35) Cundy, C. S.; Cox, P. A. *Microporous Mesoporous Mater.* **2005**, *82*, 1.
- (36) Barrer, R. M. *Zeolite Synthesis*; American Chemical Society: Washington, DC, 1989; Vol. 398, p 11.
- (37) Auerbach, S. M.; Carrado, K. A.; Dutta, P. K. *Handbook of Zeolite Science and Technology*; CRC Press: Boca Raton, FL, 2003.